



Shahid Chamran  
University of Ahvaz

# Journal of Applied and Computational Mechanics



Research Paper

## Entropy Analysis of Darcy-Forchheimer Model of Prandtl Nanofluid over a Curved Stretching Sheet and Heat Transfer Optimization by ANOVA-Taguchi Technique

B. Nagaraja<sup>1</sup>, B.J. Gireesha<sup>2</sup>, F. Almeida<sup>1</sup>, P. Kumar<sup>1</sup>, A.R. Ajaykumar<sup>1</sup>

<sup>1</sup> Department of Mathematics, School of Engineering, Presidency University, Rajanakunte, Yelahanka, Bengaluru-560064, Karnataka, India  
Email: nagaraj.kalapannahalli@gmail.com (B.N.); felcitalmeida@gmail.com (F.A.); pradimath@gmail.com (P.K.); ajayabhi219@gmail.com (A.R.A.)

<sup>2</sup> Department of Mathematics, Kuvempu University, Jnanasahyadri, Shankarghatta, Shivamogga-577451, India, Email: bjgireesu@gmail.com

Received August 10 2023; Revised November 07 2023; Accepted for publication November 08 2023.

Corresponding author: P. Kumar (pradimath@gmail.com)

© 2023 Published by Shahid Chamran University of Ahvaz

**Abstract.** Darcy-Forchheimer model has been used to consider the mathematical and statistical aspects of Prandtl nanofluid flow on a stretched curvy geometry, with homogenic-heterogenic reactions, nonlinear radiation, exponential heat, Joule heating, velocity slip, and convective heat conditions. An account of entropy significance has been given to boost the applicability of the study. The 4-5<sup>th</sup> ordered numerical tool, Runge-Kutta-Fehlberg, has been employed to establish the plots for the considered flow. ANOVA and Taguchi optimisation technique is used to obtain the optimal condition in enhancing the heat transfer rate for modelled mathematical problem. Here, the study reveals that the increasing homo-heterogenic strength parameters foster the concentration profile. The study also found that the thermal curves are positively affected by the radiation parameter and the temperature differential parameter. In addition to this, graphical portraits of isotherms and streamlines have been given to characterise the flow and heat pattern. Taguchi method reveal that first level of Prandtl number, magnetic parameter, Weissenberg number, heat source parameter and third level of curvature parameter, produce maximum Nusselt number. Heat source parameter has large contribution of about 49.45% among the other parameters and Prandtl number has the least contribution of about 1.4% for optimisation.

**Keywords:** Curved stretching sheet; Prandtl nanofluid; Darcy-Forchheimer flow; convection; ANOVA and Taguchi method, homo-heterogenic reactions; entropy propagation.

### 1. Introduction

The widened applications of multiphase flow of different kinds of fluids over continuously elongated surfaces are encouraging cutting-edge research in the field. An illustration of this is the conveyance of fluid on a stretched sheet of curvy nature. The curvy nature of the stretching sheet causes a change in flow behavior with respect to the change in flow steering parameters. Many scholars all over the world have contributed useful results. Sajid et al. [1] have produced useful outcomes for the fluid stream over a curved, elongated sheet. One such important result is that the curvature factor decreases the coefficient of drag. Hayat et al. [2] have performed explorative study upon the flow mixed convective of nanofluids over an elongated, curved surface, and they have obtained convergent series solutions. Narla et al. [3] have obtained the optimization of entropy propagation in flow due to curved geometry. The study on flow of non-Newtonian model (Casson) along a curved sheet of stretching nature has been investigated by Nagaraja and Gireesha [4]. Flow of nanofluid past a curved sheet of stretching nature was conducted by Usman et al. [5], in which the magnetic dipole contributes equally constrained streamlines on the curved sheet. Khan and Alzahrani [6] have explored the flow of viscous fluid over curved geometry, and they have discussed the important outcomes of the study.

The expansive research by taking considerations of non-Newtonian models caters much to modern industrial needs. In particular, non-Newtonian nanofluids flow over continuously stretching surface. It has many applications in firefighting materials, cement industry, mud drilling, shampoos and solution of sugar etc., Hence, non-Newtonian fluid flows are the topic worth analyzing. Prandtl fluid is classified as a shear thinning non-Newtonian fluid. Researchers have scrutinized this fluid flow model in replication of flow of blood. Nadeem et al. [7] analyzed blood flow implementing Prandtl fluid paradigm and concluded that stenosis shape parameter depletes the velocity profile. The research conducted by Khan et al. [8] looked at the fluid when there were homogeneous and



heterogeneous chemical processes on a stretched surface. Hamid et al. [9] looked at the Prandtl model's transient flow in the presence of urgent effects and found that low Reynolds numbers have big effects on velocity. Cattaneo-Christov heat flux for the Prandtl fluid was investigated by Salmi et al [10]. They have deduced that Ohmic dissipation for Ag-Prandtl fluid is weaker than that of Ag-Fe<sub>3</sub>O<sub>4</sub>-Prandtl fluid. Patil et al [11] examined the dual diffused flow of Prandtl model through a tilt permeable surface. Thermal boundary layer escalates on increasing Dufour number and unsteadiness parameter.

Darcy's model is a relation which portrays the stream of fluid in a porous media. It is being used in many industrial applications, like petroleum engineering aquifers, coffee brewing, and many more. In the presence of inertial forces and in the absence of gravitational forces, the law is modified as Darcy-Forchheimer law. Hayat et al. [12] examined how the Darcy-Forchheimer framework affected the flow generated due to the stretching of curved sheet. The skin coefficient of friction increases with inertial values. Giresha et al. [13] considered the Darcy-Forchheimer connection when studying CNT flow over a stretched surface of curvy feature. Muhammad et al. [14] investigated the Darcy-Forchheimer double diffusive flow across an exponentially curved long sheet. Synthesizing the entropy propagation of the Darcy Forchheimer flow over curved geometry, Muhammad et al. [15] to the conclusion that this phenomenon increases the inertial factor.

The electromagnetic radiation converted from thermal radiation emitted by the movement of fluids, has practical applications in thermal power plants, automobile radiators, solar energy products and so on. It has been found by Hayat et al. [16] that the thermal difference factor increases the thermal panel of the flow of Oldroyd-B model driven by melting sheet which is allowed to stretch continuously. Consequences of nonlinear thermal emission along with allied effects on micropolar fluid upon the surface when it is allowed stretch nonlinearly, which was conducted by Patel and Singh [17]. They have inferred that the Nusselt number diminishes with an upsurge in the nonlinear radiation element. Raza et al. [18] have scrutinized the radiative flow of Williamson model past a curved elongating geometry in their study. Algehyne et al. [19] have undertaken comparative research on the flow of Oldroyd-B and Casson fluid models embedded in a stratified stretched sheet.

Numerous chemically reactive structures contain homo-heterogenic reactions, viz. biochemical systems, combustion, and catalysis. The interrelation among homo-heterogenic forms of reactions is an absolute complex. Imtiaz et al. [20] have incurred the homo-heterogenic reactions effect on the transient flow over curved surface. They have concluded that concentration distribution depletes for the homogenic reaction element and enhances for the heterogenic reaction element. Pal and Mandal [21] studied the homo-heterogenic reactions influence on CNTs nanofluid flow over a stretched plate. Many other scholars [22-23] have considered the study on different fluids' flow over stretching surface of curvy feature under the effects of on homo-heterogenic reactions. Velocity slip condition and convective mode of thermal and solutal transfer through the boundary of stretching geometry have significant consequences on the flow of different fluids. Several authors [24-27] have explored the same boundary conditions in their research studies. They have come up with interesting findings about the impacts of the mentioned conditions.

The propagation of heat inside the flow structure is personified as heat propagation. This propagation is sometimes accelerated exponentially by the rapid movement of fluid particles. Animasaun et al. [28] analyzed Casson model flow upon a surface with exponential stretch, envisioning the effect of exponentially depleting heat propagation, and recorded that the thermal propagation pace is enhanced for whopping Marangoni convection. Soret and Dufour elements negatively affect concentration regimes, as explored by Zia et al. [29], who considered the effect of exponential heat on the flow of Casson model by a sheet with melting nature. Kumar et al. [30] studied MHD flow over a melted sheet having exponential heat and discovered that the melting factor inversely affects flow contours. The authors [31-32] have investigated the heat generation impacts on flow over curved geometries.

The fabrication of a system that provides productive efficiency is of prime priority among researchers. This potential design can be contrived when loss due to friction as well as heat hits the rock bottom. A fruitful manner of achieving this is by going through the concept of how entropy is produced and how it can be optimized. This irreversibility can be reported with the aid of the thermodynamic second law, which numerically formulates entropy in a sophisticated manner. Whenever, higher the entropy generated lower is the system efficiency. Therefore, the irreversibilities borne of the system need to be fewer. Initially, Bejan [33] made an attempt to analyze the entropy produced and the effectual way of minimalizing entropy. Furthering this concept made an unexpected encroachment by following researchers. Hayat et al. [34] conducted a computational scrutiny of the entropy produced when partial slip effects are anticipated at the boundary. Diminishing Bejan number was perceived by them for magnified Brinkman number. Almeida et al. [35] emphasized the irreversibility of production in the stretching channel under the influence of squeezing flow. They have disclosed that the Bejan number panel deciphers lesser irreversibility due to heat transfer. Mishra et al. [36] gave away the outcomes for irreversibility caused when the Darcy-Forchheimer paradigm was implemented in the presence of homo-heterogenic reactions. Their study reports a reduction in entropy for improved permeability values. Almeida et al. [37] scrutinized entropy in the microchannel of low aspect ratio for the flow of Al<sub>2</sub>O<sub>3</sub>-H<sub>2</sub>O when subjected to a magnetic field's pull or influence. The outcome of their study has revealed that magnification of the activation energy parameter causes depletion in exetetic effectiveness. Recently, Sheikholeslami et al. [38-40] have given the important contributions with significant outcomes in the field. In the same way many scholars [41-47] have given very innovative advancement in the field. Many other researchers [48-52] have analyzed entropy under different conditions and obtained significant results.

With the above wide range of studies, the essence of the present study is to analyze the Darcy-Forchheimer flow of Prandtl nanofluid over curved surface which is allowed to stretch under different circumstances. Here, the flow is deliberated by the stretching of convective and slippery curved sheet. Generation of entropy has been studied explicitly along with graphical portraits. In the above literature review, no studies came up with innovative optimization techniques. Hence, we have conducted optimization study for the thermal transfer pace using ANOVA and Taguchi method. We have identified the key factors effecting Nusselt number through which optimization can be done.

## 2. Mathematical Articulation

Consider the Prandtl nanofluid flow and the MHD, steady state flow is propelled by a stretched sheet of curvy nature. By fixing the origin and normalizing the  $r$ -orientation, two opposing pressures along the  $s$ -orientation stretch the sheet over a semicircle having radius  $R$  [see Fig. 1]. Let  $u_w(s) = as$  be the stretching pace of the sheet. The Darcy-Forchheimer model is contemplated to study the flow and thermal features of the said nanofluid.  $B_0$ , the magnetic field strength is acted in parallel with the  $r$ -orientation. In the energy equation, the effects of an exponentially generating thermal source as well as nonlinear radiation are considered to analyze the thermal transmission rate. The boundary of the surface is enriched with the effects of slip and convection. The no-slip condition can be studied



by taking  $L_{slip} = 0$ . The chemical samples A and B with homo-heterogenic reactions of respective concentrations  $C_a$  and  $C_b$ , are considered to discuss the mass transfer operation. The homogenic reaction on the driving sheet is  $A + 2B \rightarrow 3B$  with  $k_c C_a C_b^2$  rate  $k_s C_a$  be the rate of heterogenic reaction on the same.

With all the mentioned presumptions, following mathematical modelling has been constructed [46, 47]:

$$\frac{\partial}{\partial r} \{ (r + R)v \} + R \frac{\partial u}{\partial s} = 0, \tag{1}$$

$$\frac{\rho u^2}{r + R} = \frac{\partial p}{\partial r}, \tag{2}$$

$$v \frac{\partial u}{\partial r} + \left( \frac{Ru}{r + R} \right) \frac{\partial u}{\partial s} + \frac{uv}{r + R} = -\frac{1}{\rho} \left( \frac{R}{r + R} \right) \frac{\partial p}{\partial s} + \nu \frac{A_p}{C_p} \left( \frac{\partial^2 u}{\partial r^2} + \frac{1}{r + R} \frac{\partial u}{\partial r} - \frac{u}{(r + R)^2} \right) - Fu^2 - \frac{\nu}{k_p} u - \frac{\sigma}{\rho} B_0^2 u + \tag{3}$$

$$+ \nu \frac{A_p}{2C_p^3} \left\{ \left( \frac{\partial u}{\partial r} \right)^2 \frac{\partial^2 u}{\partial r^2} + \frac{1}{r + R} \left[ \left( \frac{\partial u}{\partial r} \right)^3 - 2u \frac{\partial u}{\partial r} \frac{\partial^2 u}{\partial r^2} \right] + \frac{u}{(r + R)^2} \left[ \frac{u}{(r + R)^2} \frac{\partial^2 u}{\partial r^2} - 3 \left( \frac{\partial u}{\partial r} \right)^2 \right] + \frac{3u^2}{(r + R)^3} \frac{\partial u}{\partial r} - \frac{u^3}{(r + R)^4} \right\},$$

$$v \frac{\partial T}{\partial r} + \left( \frac{R}{r + R} \right) u \frac{\partial T}{\partial s} = \alpha \left( \frac{\partial^2 T}{\partial r^2} + \frac{1}{r + R} \frac{\partial T}{\partial r} \right) + \frac{\nu}{c_p} \left[ \frac{A_p}{C_p} \left( \frac{\partial u}{\partial r} - \frac{u}{r + R} \right)^2 + \frac{A_p}{2C_p^3} \left( \frac{\partial u}{\partial r} - \frac{u}{r + R} \right)^4 \right] + \tag{4}$$

$$+ \tau \left[ D_{c_a} \left( \frac{\partial C_a}{\partial r} \frac{\partial T}{\partial r} \right) + \frac{D_T}{T_\infty} \left( \frac{\partial T}{\partial r} \right)^2 \right] - \frac{1}{\rho c_p} \frac{1}{r + R} \frac{\partial \{ (r + R)q_r \}}{\partial r} + \frac{Q_0}{\rho c_p} (T - T_\infty) e^{(-\sqrt{a}r/r)} + \frac{\sigma}{\rho c_p} B_0^2 u^2,$$

$$v \frac{\partial C_a}{\partial r} + \frac{R}{(r + R)} u \frac{\partial C_a}{\partial s} = D_{c_a} \left( \frac{\partial^2 C_a}{\partial r^2} + \frac{1}{r + R} \frac{\partial C_a}{\partial r} \right) + \frac{D_T}{T_\infty} \left( \frac{\partial^2 T}{\partial r^2} + \frac{1}{r + R} \frac{\partial T}{\partial r} \right) - k_c C_a C_b^2, \tag{5}$$

$$v \frac{\partial C_b}{\partial r} + \frac{R}{(r + R)} u \frac{\partial C_b}{\partial s} = D_{c_b} \left( \frac{\partial^2 C_b}{\partial r^2} + \frac{1}{r + R} \frac{\partial C_b}{\partial r} \right) + \frac{D_T}{T_\infty} \left( \frac{\partial^2 T}{\partial r^2} + \frac{1}{r + R} \frac{\partial T}{\partial r} \right) + k_c C_a C_b^2, \tag{6}$$

The related peripheral conditions are [22, 23]:

$$u = as + L_{slip} \left[ \frac{\partial u}{\partial r} - \frac{u}{r + R} \right], v = 0, -k \frac{\partial T}{\partial r} = h_1 (T_w - T), D_{c_a} \frac{\partial C_a}{\partial r} = k_s C_a, D_{c_b} \frac{\partial C_b}{\partial r} = -k_s C_b \text{ at } r = 0, \tag{7}$$

$$u \rightarrow 0, v \rightarrow 0, \frac{\partial u}{\partial r} \rightarrow 0, T \rightarrow T_\infty, C_a \rightarrow C_0, C_b \rightarrow 0 \text{ as } r \rightarrow \infty.$$

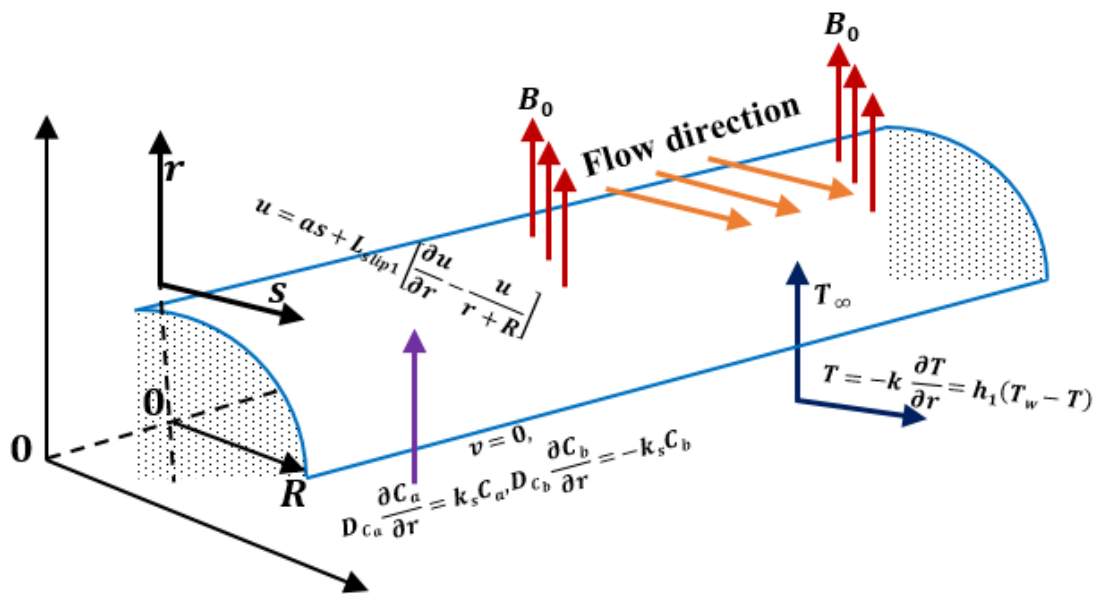


Fig. 1. Pictorial demonstration of considered flow.



Here, velocities ( $u, v$ ) along ( $s, r$ )-orientations, pressure, density, kinematic viscosity, material constants of Prandtl Fluid, permeability of porous medium, non-uniform inertia coefficient of porous medium, electrical conductivity, magnetic field intensity, thermal diffusivity, specific heat, temperature, effective heat capacity ratio, space dependent heat source, nonlinear radiative heat flux, ambient fluid temperature, diffusive coefficient of A, diffusive coefficient of B, thermophoretic diffusion coefficient, rate constant, velocity slip coefficient, convective heat transport coefficient, temperature of the fluid at the surface, thermal conductivity, and rate constant are resembled by pseudonyms  $p, \rho, \nu, (A_p \& C_p), k_p, F, \sigma, B_0, \alpha, c_p, T, \tau, Q_0, q_r, T_\infty, D_{ca}, D_{cb}, D_T, k_c, L_{slip}, h_1, T_w, k$  and  $k_s$ , respectively.

The approximated nonlinear form of radiative heat flux by Rosseland is as below:

$$q_r = -\frac{4\sigma^*}{3k^*} \frac{\partial T^4}{\partial r} = \left( -\frac{16\sigma^* T^3}{3k^*} \right) \frac{\partial T}{\partial r}, \tag{8}$$

where  $k^*$  and  $\sigma^*$  are Stefan-Boltzman constant and average absorption factor.

In order to decipher simplified version of flow steering equations, following morphing catalysts are considered:

$$u = asf'(\eta), v = \frac{-R}{r+R} \sqrt{a\nu} f(\eta), \eta = \sqrt{\frac{a}{\nu}} r, p = \rho a^2 s^2 P(\eta), \kappa = \sqrt{\frac{a}{\nu}} R, T = T_\infty [1 + (\theta_w - 1)\theta(\eta)], C_a = C_0\phi(\eta), C_b = C_0h(\eta) \tag{9}$$

where  $f'(\eta), \theta(\eta), P(\eta), h(\eta)$  and  $\phi(\eta)$  are sequentially the velocity, temperature, pressure, heterogenic and homogenic concentration regimes which are all of dimension 1. Prime resembles derivative with respect to  $\eta$  (cohesive variable),  $\theta_w$  is the temperature ratio element,  $\kappa$  is the dimensionless parameter of curvature, and  $C_0$ -the constant.

Equation (1) is adequately satisfied and relations (2) to (6) yield:

$$\frac{\partial P}{\partial \eta} = \frac{f'^2}{\eta + \kappa}, \tag{10}$$

$$\begin{aligned} \frac{2\kappa}{\eta + \kappa} P = & \frac{\kappa}{\eta + \kappa} fff'' - \frac{\kappa}{\eta + \kappa} f'^2 + \frac{\kappa}{(\eta + \kappa)^2} fff' + \alpha_p \left[ f''' + \frac{1}{\eta + \kappa} f'' - \frac{1}{(\eta + \kappa)^2} f' \right] + \\ + \beta_p \left[ f''^2 f''' - \frac{1}{\eta + \kappa} (2ff''f''' - f'''^3) - \frac{1}{(\eta + \kappa)^2} (3ff''^2 - f'^2 f''') + \frac{3}{(\eta + \kappa)^3} f'^2 f'' - \frac{1}{(\eta + \kappa)^4} f'^3 \right] - Frf'^2 - \lambda f' - Mf', \end{aligned} \tag{11}$$

$$\begin{aligned} \frac{1}{Pr} \left[ 1 + \{1 + (\theta_w - 1)\theta\}^3 Rd \right] \left[ \theta'' + \frac{1}{\eta + \kappa} \theta' \right] + \frac{3Rd}{Pr} [1 + (\theta_w - 1)\theta]^2 (\theta_w - 1)\theta'^2 + Q\theta e^{-\eta} + \\ + Ec \left[ \alpha_p \left( f'' - \frac{f'}{\eta + \kappa} \right)^2 + \beta_p \left( f'' - \frac{f'}{\eta + \kappa} \right)^4 \right] + \frac{\kappa}{\eta + \kappa} f\theta' + Nb\theta'\phi' + Nt\theta'^2 + MEcf'^2 = 0, \end{aligned} \tag{12}$$

$$\frac{1}{Sc} \left[ \frac{\phi'}{\eta + \kappa} + \phi'' \right] + \frac{\delta Nt}{Sc Nb} \left[ \theta'' + \frac{1}{\eta + \kappa} \theta' \right] + \frac{\kappa}{\eta + \kappa} f\phi' - k_1\phi h^2 = 0, \tag{13}$$

$$\frac{\delta}{Sc} \left[ \frac{h'}{\eta + \kappa} + h'' \right] + \frac{\delta Nt}{Sc Nb} \left[ \theta'' + \frac{1}{\eta + \kappa} \theta' \right] + \frac{\kappa}{\eta + \kappa} fh' + k_1\phi h^2 = 0. \tag{14}$$

The transfused boundary conditions are:

$$f' = 1 + Ls \left[ f''(0) - \frac{f'(0)}{\kappa} \right], f = 0, \theta' = -Bi[1 - \theta(0)], \phi' = k_2\phi(0), \delta h' = -k_2\phi(0) \tag{15}$$

$$f' \rightarrow 0, f'' \rightarrow 0, \theta \rightarrow 0, \phi \rightarrow 1 \text{ as } \eta \rightarrow \infty,$$

where  $\alpha_p(= A_p / C_p)$ -Prandtl fluid parameter,  $\beta_p(= a^3 s^2 A_p / 2\nu C_p^3)$ -elastic parameter,  $Fr(= Fs)$ -Forchheimer number,  $\lambda(= \nu / k_p a)$ -porous parameter,  $M(= \sigma B_0^2 / \rho a)$ -Hartman number,  $Pr(= \nu / \alpha)$ -Prandtl number,  $Rd(= 16\sigma^* T_\infty^3 / 3kk^*)$ -radiation parameter,  $Ec(= u_w^2 / [c_p T_\infty (\theta_w - 1)])$ -Eckert number,  $Nb(= \tau D_{c_0} C_0 / \nu)$ -Brownian motion parameter,  $Q(= Q_0 / [a(\rho c_p)])$ -heat source/sink parameter,  $Nt(= \tau D_T (\theta_w - 1) / \nu)$ -thermophoresis parameter,  $Sc(= \nu / D_{c_0})$ -Schmidt number,  $\delta(= D_{c_0} / D_{c_1})$ -ratio of diffusion coefficients,  $k_1(= C_0^2 k_c / a)$ -homogenic reaction parameter,  $Ls(= L_{slip} \sqrt{a} / \nu)$ -velocity slip parameter,  $Bi(= h_1 \sqrt{\nu} / a / k)$ -thermal Biot number and  $k_2(= k_s \sqrt{\nu} / a / D_{c_0})$ -heterogenic reaction parameter.

Elimination of  $P(\eta)$  from equations (10) and (11), gives:

$$\begin{aligned} \alpha_p \left[ f''^2 + \frac{2f'''}{\eta + \kappa} - \frac{f''}{(\eta + \kappa)^2} + \frac{f'}{(\eta + \kappa)^3} \right] + \frac{\kappa}{\eta + \kappa} [fff''' - f'f'''] + \frac{\kappa}{(\eta + \kappa)^2} [fff'' - f'^2] - \frac{\kappa}{(\eta + \kappa)^3} fff' + \\ + \beta_p \left[ (f''^2 f''^2 + 2ff''f''^2) - \frac{2}{\eta + \kappa} (ff''f''^2 + fff''f''^2 - f''^2 f''') - \frac{1}{(\eta + \kappa)^2} (3f''^3 + 4ff''f''^2 - f'^2 f''^2) + \frac{1}{(\eta + \kappa)^3} (2f'^2 f''^2 + 9ff''f''^2) - 9 \frac{f'^2 f''}{(\eta + \kappa)^4} + 3 \frac{f'^3}{(\eta + \kappa)^5} \right] - \\ - Fr \left[ 2ff'' + \frac{f'^2}{\eta + \kappa} \right] - \lambda \left[ f'' + \frac{f'}{\eta + \kappa} \right] - M \left[ f'' + \frac{f'}{\eta + \kappa} \right] = 0 \end{aligned} \tag{16}$$



when  $D_{c_a} = D_{c_b}$  then  $\delta = 1$  and  $\phi(\eta) + h(\eta) = 1$ . Now Eqs. (13) and (14) yield:

$$\frac{1}{Sc} \left[ \frac{\phi'}{\eta + \kappa} + \phi'' \right] + \frac{\kappa}{\eta + \kappa} f \phi' - k_1 \phi (1 - \phi)^2 = 0, \tag{17}$$

along with boundary constraints:

$$\phi'(0) = k_2 \phi(0), \quad \phi(\infty) \rightarrow 1. \tag{18}$$

The attributes of engineering prominence are dragging factor and Nusselt number which are stated by:

$$Cf_s = \frac{\tau_{rs}}{\rho u_w^2}, Nu_s = \frac{Sq_w}{kT_\infty (\theta_w - 1)}, \tag{19}$$

where  $\tau_{rs}$  and  $q_w$  are stress and heat near the wall, respectively, and are expressed by:

$$\tau_{rs} = \mu \left[ \frac{A_p}{C_p} \left( \frac{\partial u}{\partial r} - \frac{u}{r+R} + \left( \frac{R}{R+r} \right) \frac{\partial v}{\partial s} \right) + \frac{A_p}{6C_p^3} \left( \frac{\partial u}{\partial r} - \frac{u}{r+R} + \left( \frac{R}{R+r} \right) \frac{\partial v}{\partial s} \right)^3 \right] \Bigg|_{r=0}, \tag{20}$$

$$q_w = -k \left( \frac{\partial T}{\partial r} \right) \Bigg|_{r=0} + q_r \Big|_{r=0}. \tag{21}$$

The transfused forms of above expressions are:

$$Cf_s (Re)^{\frac{1}{2}} = \alpha_p \left[ f''(0) - \frac{1}{\kappa} f'(0) \right] + \frac{\beta_p}{3} \left[ f''(0) - \frac{1}{\kappa} f'(0) \right]^3 \tag{22}$$

$$Nu_s (Re)^{-\frac{1}{2}} = - \left[ 1 + \{ 1 + (\theta_w - 1) \theta \}^3 Rd \right] \theta'(0), \tag{23}$$

where  $Re = as^2 / \nu$  denotes local Reynolds number.

### 3. Entropy Generation

The entropy produced in flow driven by curved sheet of stretching feature with irreversibility of porous medium heat transmission, viscous dissipation, Joule heating and mass transmission is given by:

$$E_g = \frac{k}{T_\infty^2} \left\{ 1 + \frac{16\sigma^* T^3}{3k^*} \right\} \left( \frac{\partial T}{\partial r} \right)^2 + \frac{\mu}{T_\infty} \left[ \frac{A_p}{C_p} \left( \frac{\partial u}{\partial r} - \frac{u}{r+R} \right)^2 + \frac{A_p}{2C_p^3} \left( \frac{\partial u}{\partial r} - \frac{u}{r+R} \right)^4 \right] + \frac{Fu^3}{T_\infty} + \frac{\mu u^2}{T_\infty k_p} + \frac{\sigma B_0^2 u^2}{T_\infty} + \frac{RD_{c_a}}{T_\infty} \left( \frac{\partial C_a}{\partial r} \frac{\partial T}{\partial r} \right) + \frac{RD_{c_a}}{C_a} \left( \frac{\partial C_a}{\partial r} \right)^2 + \frac{RD_{c_b}}{T_\infty} \left( \frac{\partial C_b}{\partial r} \frac{\partial T}{\partial r} \right) + \frac{RD_{c_b}}{C_b} \left( \frac{\partial C_b}{\partial r} \right)^2 \tag{24}$$

Dimensionless form of entropy generation is:

$$Ng = \alpha_1 \left\{ 1 + (1 + (\theta_w - 1) \theta)^3 Rd \right\} \theta'^2 + Br \left[ \alpha_p \left( f'' - \frac{f'}{\eta + \kappa} \right)^2 + \beta_p \left( f'' - \frac{f'}{\eta + \kappa} \right)^4 \right] + Br \left[ (M + \lambda) f'^2 + Fr f'^3 \right] + (L_1 - L_2) \theta' \phi' + \left( \frac{L_1}{\phi} + \frac{L_2}{1 - \phi} \right) \frac{\phi'^2}{\alpha_1} = 0, \tag{25}$$

where  $Ng(= \nu E_g / ak(\theta_w - 1))$  -total entropy,  $\alpha_1(= \theta_w - 1)$  -temperature ratio parameter,  $Br(= \mu a^2 s^2 / [T_\infty (\theta_w - 1)k])$  - Brinkman number,  $L_1(= RD_{c_a} C_0 / k)$  -homogenic diffusion parameter and  $L_2(= RD_{c_b} C_0 / k)$  -heterogenic diffusion parameter.

Bejan number is defined as follows:

$$Be = \frac{\alpha_1 \left\{ 1 + (1 + (\theta_w - 1) \theta)^3 Rd \right\} \theta'^2 + (L_1 - L_2) \theta' \phi' + \left( \frac{L_1}{\phi} + \frac{L_2}{1 - \phi} \right) \frac{\phi'^2}{\alpha_1}}{\alpha_1 \left\{ 1 + (1 + (\theta_w - 1) \theta)^3 Rd \right\} \theta'^2 + Br \left[ \alpha_p \left( f'' - \frac{f'}{\eta + \kappa} \right)^2 + \beta_p \left( f'' - \frac{f'}{\eta + \kappa} \right)^4 \right] + Br \left[ (M + \lambda) f'^2 + Fr f'^3 \right] + (L_1 - L_2) \theta' \phi' + \left( \frac{L_1}{\phi} + \frac{L_2}{1 - \phi} \right) \frac{\phi'^2}{\alpha_1}} \tag{26}$$

### 4. Results and their Deliberation

The mathematical contemplation of Darcy-Forchheimer modelling of a Prandtl nanofluid stream driven by a stretched surface of curvy nature. The configured equations under the stated effects are switched to simple equations by utilizing similarity catalysts. Runge-Kutta-Fehlberg 4-5<sup>th</sup> order method, an efficient numerical tool, is availed to portray graphical representations for the considered flow problem. Other parameters were set to  $Bi = 0.1, Ec = 0.1, Fr = 0.1, \lambda = 1, Ls = 1, M = 0.5, Nb = 0.01, Nt = 0.01, Pr = 7, Q = 0.1, Rd = 0.5, Sc = 5, \theta_w = 2, \alpha_p = 2, \beta_p = 6, \kappa = 5, k_1 = 0.1, k_2 = 0.1$  while extracting numerical graphs for all flow regimes. Validation of the current method is correlated with the NDSolve technique attained by Hayat et al. [34] in table 1 and both the results show good synergy. A prolonged discussion has been given below for the extracted graphs.



**Table 1.** Correlation of current sample data and existing sample data.

$\kappa$	$Fr$	$\lambda$	$f''(0) - f'(0) / \kappa$ [34]	$f''(0) - f'(0) / \kappa$ [Present]
0.7	0.1	0.1	3.20889	3.208887
0.8			2.88705	2.887054
0.9			2.64211	2.642109
0.9	0.0		2.60608	2.606084
	0.1		2.64211	2.642109
	0.2		2.67674	2.676735
	0.1	0.0	2.57554	2.575537
		0.1	2.64211	2.642109
		0.2	2.70364	2.703640

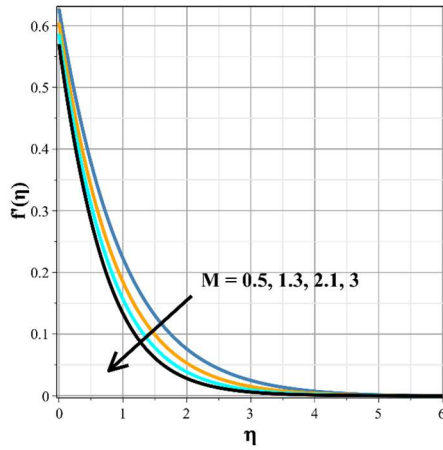


**Fig. 2.** Velocity  $f'(\eta)$  curves for  $M$ .

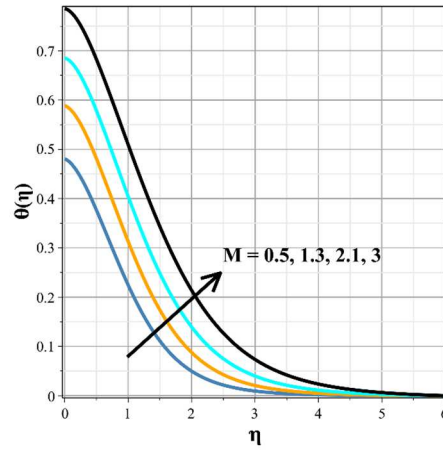


**Fig. 3.** Thermal  $\theta(\eta)$  curves for  $M$ .

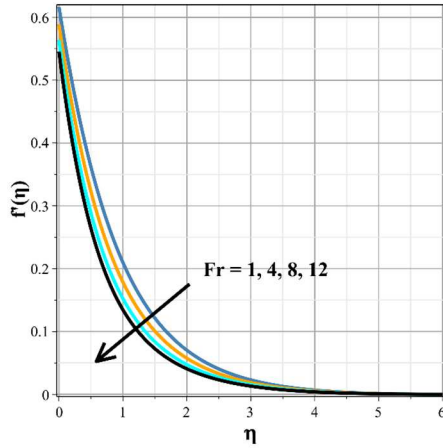


**Fig. 4.** Velocity  $f'(\eta)$  curves for  $Fr$ .

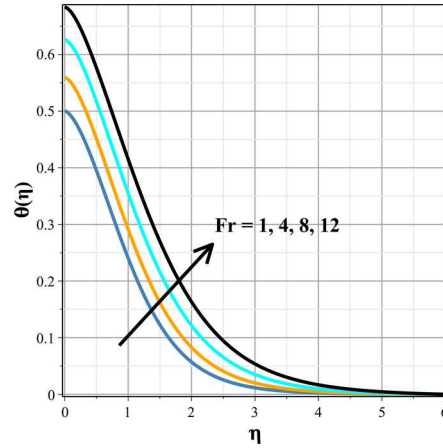


**Fig. 5.** Thermal  $\theta(\eta)$  curves for  $Fr$ .

Figure 2 lucidly showcases the fluctuations of velocity panel ( $f'(\eta)$ ) for upsurging magnitude of the magnetic attribute ( $M$ ) which is descending in nature. This impedance of velocity is attributed to the Lorentz force, which is enhanced by the rise of  $M$  whereas, it reciprocates the trend in temperature panel as depicted in Fig. 3. Figures 4 and 5 are portrayed to characterize the impact of increasing the Forchheimer number ( $Fr$ ) on concerned panels. An upsurge in the values of the ( $Fr$ ), slows down the flow velocity panel ( $f'(\eta)$ ) as it induces pressure drop borne by fluid-solid interaction as depicted in Fig. 4. On the other hand, the temperature panel ( $\theta(\eta)$ ) ascends for the same  $Fr$  as it magnifies the thermal boundary thickness, which is exhibited in Fig. 5.

The outcome of whopping magnitude of the porous factor ( $\lambda$ ) on flow defining profile is sketched in Fig. 6. Here, the flow is deliberated through porous media and whence the fluid flows through the pores of sheet, pace of the flow reduces gradually. Figure 7 introspect the consequences of incrementing values of elastic parameter ( $\beta_p$ ) on velocity regimes. When the elasticity of the medium magnifies the speed of the fluid flourishes. Therefore, with the enhancement in elastic parameter we have perceived enhancement in the fluid velocity.





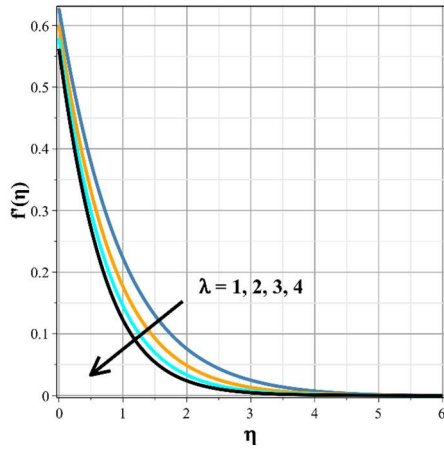


Fig. 6. Velocity  $f'(\eta)$  curves for  $\lambda$ .

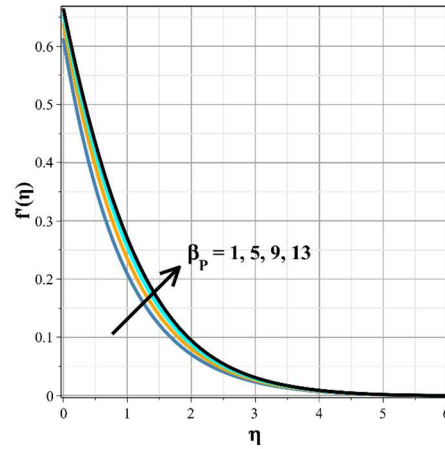


Fig. 7. Velocity  $f'(\eta)$  curves for  $\beta_p$ .

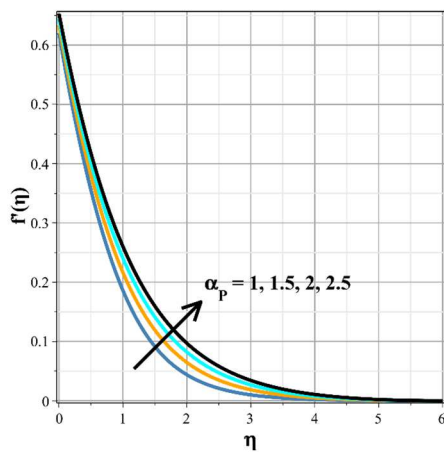


Fig. 8. Velocity  $f'(\eta)$  curves for  $\alpha_p$ .

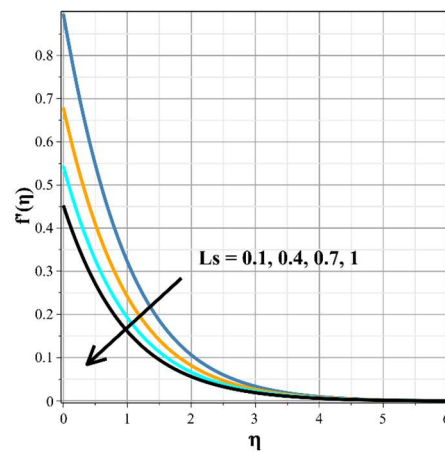


Fig. 9. Velocity  $f'(\eta)$  curves for  $L_s$ .

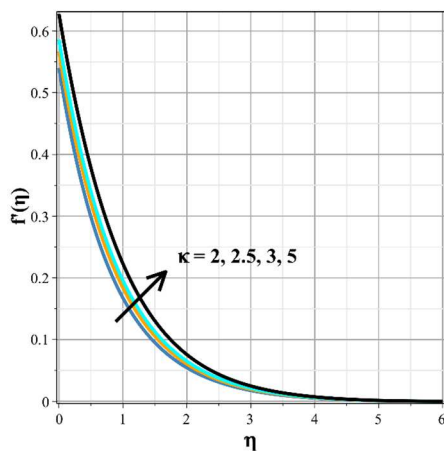


Fig. 10. Velocity  $f'(\eta)$  curves for  $\kappa$ .

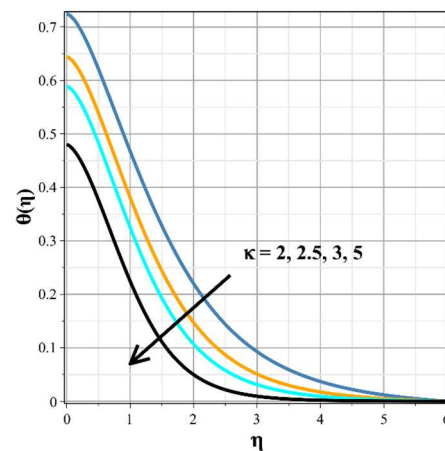


Fig. 11. Thermal  $\theta(\eta)$  curves for  $\kappa$ .

The characteristic changes in flow profiles for an increasing Prandtl fluid parameter ( $\alpha_p$ ), have been observed in Fig. 8. In Fig. 8, one can easily observe that the velocity panel escalates for escalating values of ( $\alpha_p$ ), because of the improvement of the momentum boundary layer. Figure 9 is outlined to discern the significant changes in all flow panels in variations with the velocity slip parameter ( $L_s$ ). The burgeoning values of ( $L_s$ ) exerts partial velocity on the fluid flow and impede the flow pace, which reduces the velocity panel.

Figures 10 and 11 are outlined to discern the characteristic variations of curvature parameter ( $\kappa$ ). The curved geometry's radius increases with ( $\kappa$ ), and fluid moves quicker with it. As shown in Fig. 10, increasing ( $\kappa$ ) promotes the velocity regime. ( $\kappa$ ) has an inverse relationship with kinematic viscosity, thus when, thermal profile weakens, as illustrated in Fig. 11.



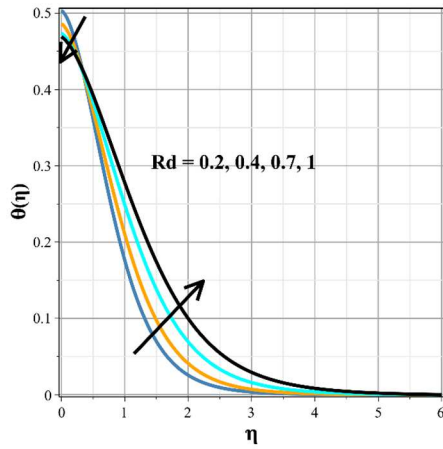


Fig. 12. Thermal  $\theta(\eta)$  curves for  $Rd$ .

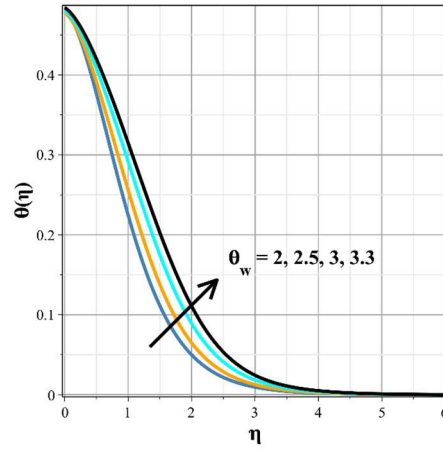


Fig. 13. Thermal  $\theta(\eta)$  curves for  $\theta_w$ .

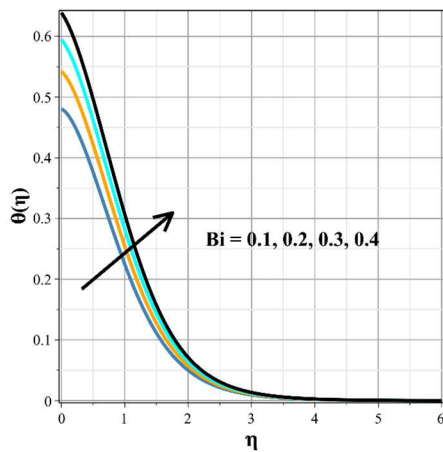


Fig. 14. Thermal  $\theta(\eta)$  curves for  $Bi$ .

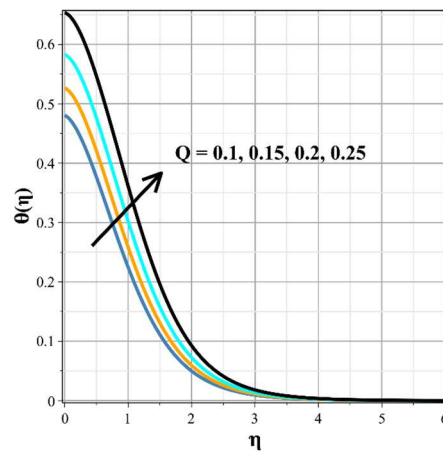


Fig. 15. Thermal  $\theta(\eta)$  curves for  $Q$ .

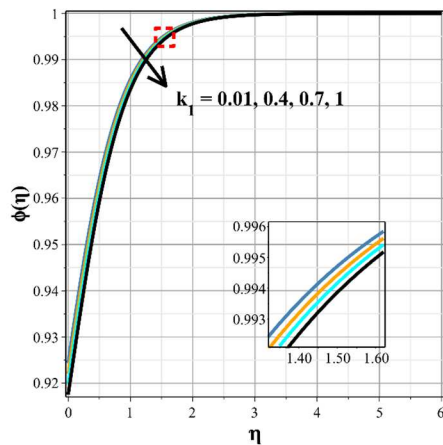


Fig. 16. Solutal  $\phi(\eta)$  curves for  $k_1$ .

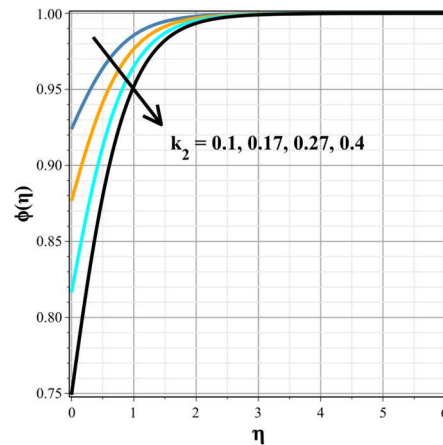


Fig. 17. Solutal  $\phi(\eta)$  curves for  $k_2$ .

Illustration of the influence of radiation factor ( $Rd$ ) on temperature panel is produced in Fig. 12. The thermal panel is flourished by the magnifying values of ( $Rd$ ) because of the reduction in mean absorption coefficient. Figure 13 shows an enhancing behavior of the thermal panel upon uplifting values of the temperature difference factor ( $\theta_w$ ). For ( $\theta_w > 0$ ), wall temperature is greater than surrounding temperature (i.e.,  $T_w > T_\infty$ ). Because of this fact, the temperature profile increases when ( $\theta_w$ ) increases. Figures 14 and 15 are respectively plotted to demonstrate variations of the thermal panel for varying heat generation element ( $Q$ ) as well as Biot number ( $Bi$ ). The thermal panel flourishes for both parameters because of the generation of heat within the fluid in the case of ( $Q$ ) and because of convective mode of heat transfer for  $Bi$ . The curves of the concentration panel for upshot values of homogenic reaction strength ( $k_1$ ) have been drawn in Fig. 16. An increase in ( $k_1$ ) discourages the concentration profile. This sort of nature is achieved because during





homogenic reaction ensues the reactants combine to form the product which implicates the consumption of reactants. Figure 17 elaborates the relationship between concentration panel and  $(k_2)$ . An increasing impact of  $(k_2)$  diminishes the mass transfer profile, as magnifying this parameter amplifies the collision frequency between reactants.

The bar depiction of entropy produced and irreversibility ratio in Figs. 18, 19 and 20 is provided for various values of  $Br$ ,  $M$  and  $Fr$ . Magnification in viscosity of the fluid magnifies the entropy generated as depicted in Fig. 18 whereas  $Be$  depletes for the amplified  $Br$  values. This is justified as the  $Br$  characterizes the viscosity of the fluid, which magnifies the disorderliness of the system. Thus, more viscous forces enhance the hindrance to the fluid flow, which means irreversibilities due to fluid friction is immense with higher  $Br$ . Hence, the irreversibilities borne of fluid friction are extreme. Response of  $M$  in Fig. 19 exemplifies augmenting nature on  $Ng$  and diminishing nature for  $Be$  which is similar to that of  $Br$  because flow is delayed with porosity which implicates higher viscosity, increasing irreversibility eventually. The bar depiction for Forchheimer number  $Fr$  is revealed in Fig. 20. Increasing  $Fr$ , has maximized the entropy of the system. Further,  $Be$  plot signifies the contrary nature to entropy, suggesting higher contributions of irreversibilities borne due to fluid friction over heat and mass transmission irreversibility.

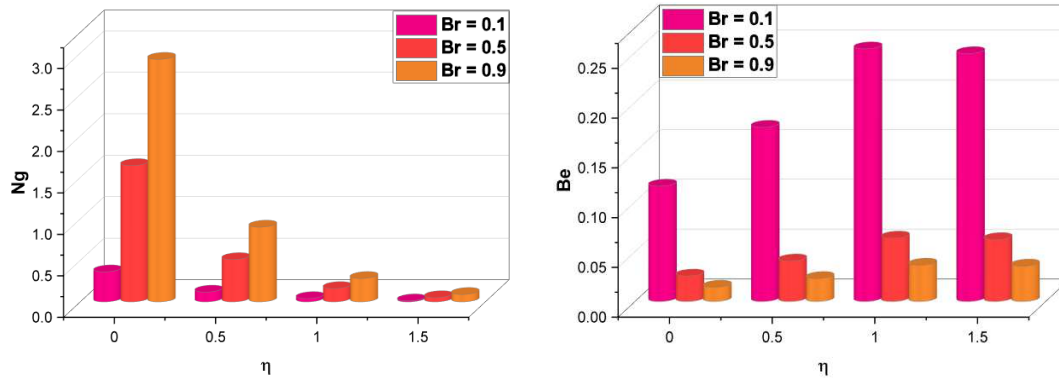


Fig. 18. Bar chart depiction of Entropy ( $Ng(\eta)$ ) and Bejan number ( $Be(\eta)$ ) for  $Br$ .

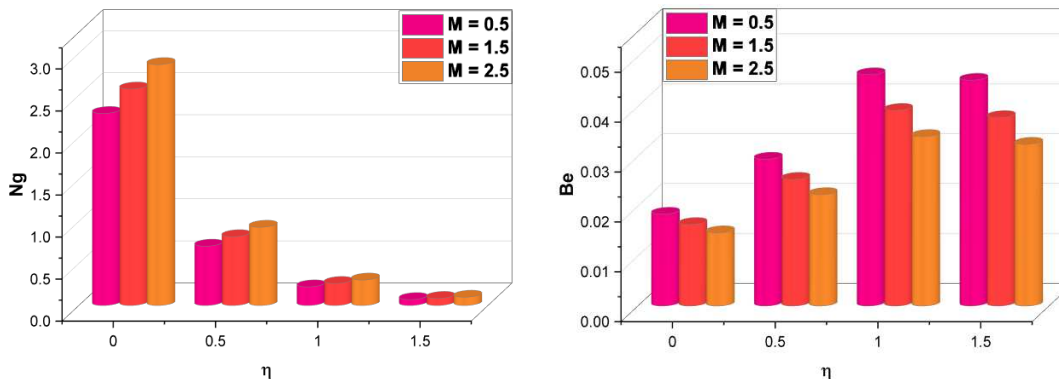


Fig. 19. Bar chart depiction of Entropy ( $Ng(\eta)$ ) and Bejan number ( $Be(\eta)$ ) for  $M$ .

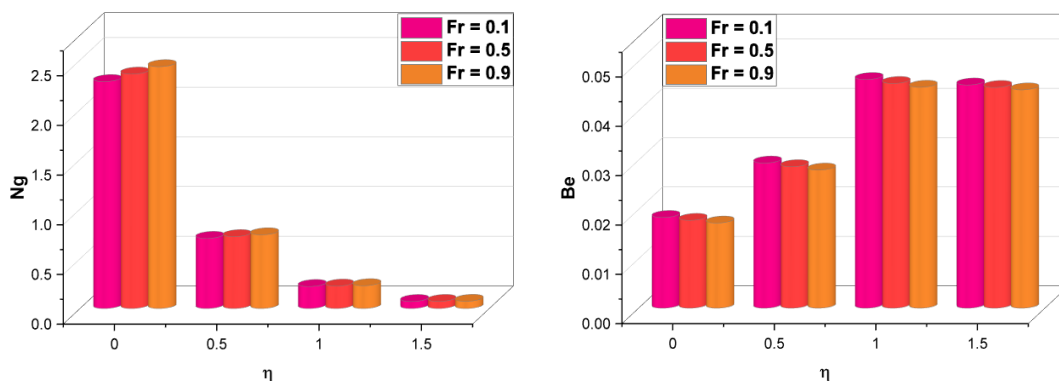


Fig. 20. Bar chart depiction of Entropy ( $Ng(\eta)$ ) and Bejan number ( $Be(\eta)$ ) for  $Fr$ .



**Table 2.** Computation values of skin-friction and Nusselt number for  $\alpha_p, \beta_p, \kappa$ .

$\alpha_p$	$\beta_p$	$\kappa$	$Cf_s(Re)^{1/2}$	$Nu_s(Re)^{-1/2}$
1	6	5	-1.27966	0.114596
1.5	6	5	-1.19995	0.119407
2	6	5	-1.13609	0.120157
2	1	5	-1.32209	0.133274
2	5	5	-1.16175	0.122851
2	9	5	-1.07534	0.111912
2	6	2.5	-1.15162	0.049203
2	6	3	-1.14172	0.082807
2	6	3.5	-1.13722	0.099768

Figure 21 elucidates the response of  $M$  against  $\lambda$  and  $Fr$  on skin friction separately. 3D illustration clearly shows that growth in  $M$  against both porous and the Forchheimer number has caused a reduction in surface drag, which suggests that a larger magnetic field on the surface can reduce drag. Figure 22 is the 3D depiction of the Nusselt number for two different parameters viz.,  $Rd$  and  $Ec$  against  $Pr$ . Figures reveal that a stronger potency of radiation over elongated sheet drains the transmission of heat when the kinematic viscosity enlarges. A similar rejoinder is perceived while studying the Nusselt number for  $Ec$  against  $Pr$  which infers that the fluid with higher viscosity has the lowest heat transport rate.

The path followed by the Prandtl fluid elements are elucidated in a 2D contour plot (streamlines) in Fig. 23 for  $M = 0.1$  and  $M = 0.9$ . A diagram with the points over a stretched surface partaking identical temperature for  $Q = 0.1$  and  $Q = 0.25$  is pictured using contours (isotherms) in Fig. 24.

Table 2 presents the values of skin-friction co-efficient and Nusselt number for various values of  $\alpha_p, \beta_p$  and  $\kappa$ . On magnifying the values of  $\alpha_p, \beta_p$  and  $\kappa$ , we can see that surface drag has magnified. Here  $\alpha_p$  and  $\beta_p$  represent the non-Newtonian characteristic of fluid and hence we observe the surface drag to magnify with these parameters. But the heat transport rate has increased for upsurging values of  $\alpha_p, \kappa$  and depleted for higher values of  $\beta_p$ .

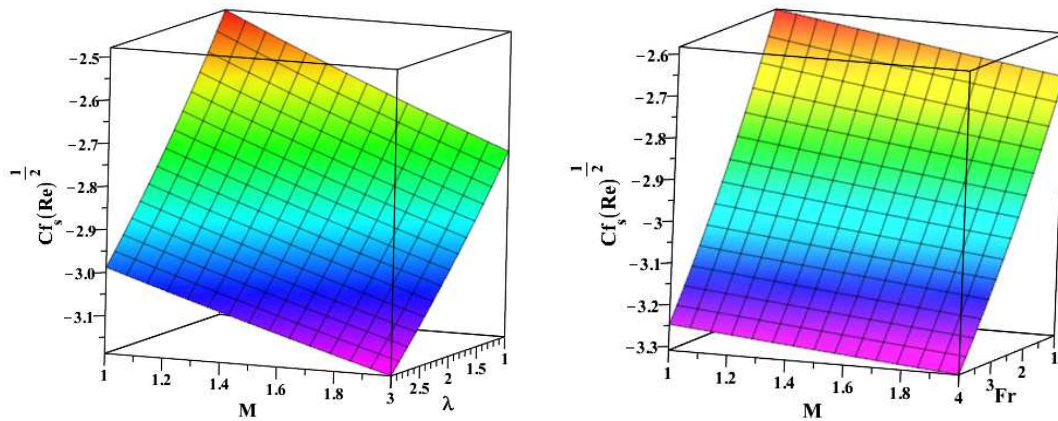


**Fig. 21.** 3D depiction of skin friction ( $Cf_s(Re)^{1/2}$ ) for  $M$  against  $\lambda$  and  $Fr$ .

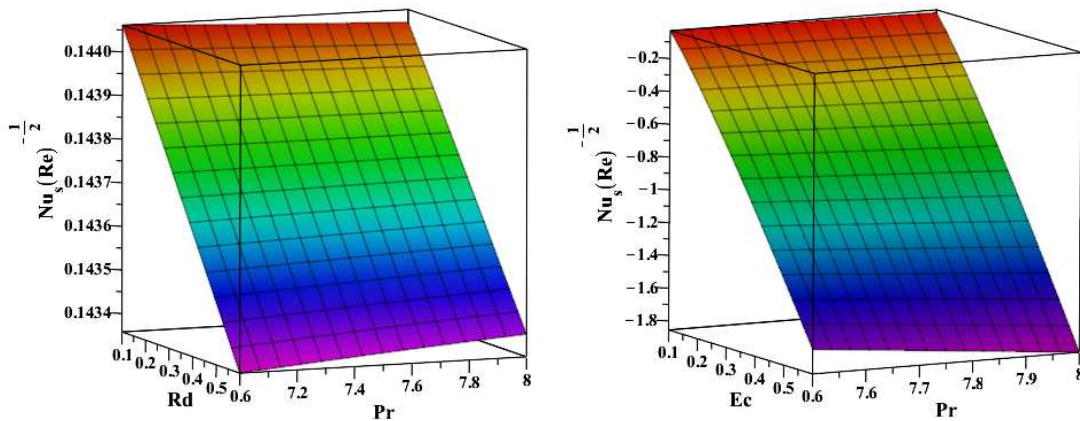


**Fig. 22.** 3D depiction of Nusselt number ( $Nu_s(Re)^{-1/2}$ ) for  $Rd$  and  $Ec$  against  $Pr$ .



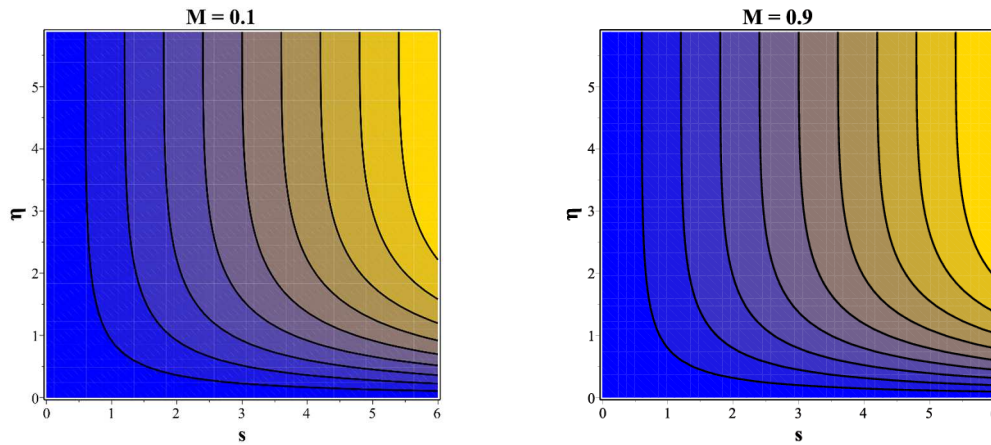


Fig. 23. Streamlines at  $M = 0.1$  and  $M = 0.9$ .

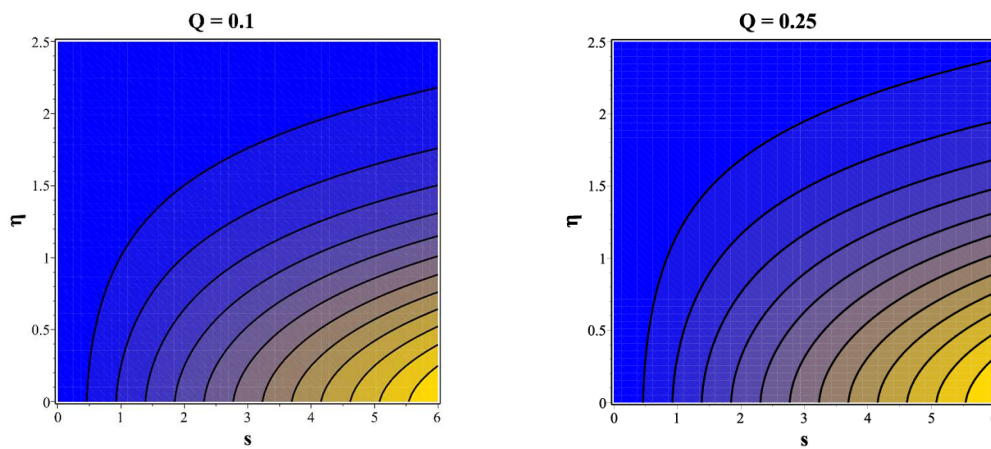


Fig. 24. Isotherms at  $Q = 0.1$  and  $Q = 0.25$ .

## 5. Optimal Theory

### 5.1. Taguchi technique

Emphasis of Taguchi tool of quality control in engineering is to design the product by reducing the defects in manufacturing process. This is a robust design developed in order to improve the standard of manufactured goods. Taguchi method makes use of orthogonal array (OA) and the orthogonal matrix has a feature that every factor fit appears the same number of times for every test fit of rest of the key factors. This helps in comparing between different factor levels for diverse conditions. The current model employs five critical factors and twenty-seven experimental runs organized in three tiers [53-56]. The appropriate signal-to-noise ratio (SNR) is generated for each parameter value set. In the current situation, the response is the Nusselt number. Magnetic parameter ( $0.1 \leq M \leq 0.7$ ), curvature parameter ( $3 \leq \kappa \leq 5$ ), elastic parameter ( $3 \leq \beta_p \leq 6$ ), Prandtl number ( $7 \leq Pr \leq 9$ ), heat source parameter ( $0.1 \leq Q \leq 0.3$ ), are the selected parameters for the Taguchi method. The various stages of considered parameters are displayed in Table 3, while their level of optimization is highlighted in Table 4. Considered is an L27 orthogonal matrix with 26 degrees of freedom. There are 125 total numerical trials in the factorial design, with three levels testing five independent key components [55]. When calculating SNR for the response variable, a larger value is considered optimal. The optimal stage of critical factors is observed at greater SNR values.

Table 5 gives the SNR responses for the different runs of experimental design. As per the Taguchi method, third level of curvature parameter ( $\kappa$ ), first level of magnetic parameter ( $M$ ), first level of elastic parameter ( $\beta_p$ ), first level of Prandtl number ( $Pr$ ) and heat source parameter ( $Q$ ) produces an optimal arrangement to obtain maximum Nusselt number as elucidated in Table 6. This is interpreted graphically in Fig. 25 which depicts that high heat transfer rate is attained for first level of  $M, Pr, \beta_p, Q$  and third level of  $\kappa$ .

### 5.2. Analysis of Variance (ANOVA) method

ANOVA is a statistical approach to compare variances across means. This is a statistical test which helps in determining whether two or more categorical groups are statistically significant on the basis of testing differences in means utilising variance. Table 7 offers the outcomes of ANOVA for response variable. The performed analysis demonstrates precision with an R-squared value of 81.15%; such values indicate that the selected model provides a decent fit. Additionally, values are considered statistically significant when the F-value is greatest and the p-value is least, specifically less than 0.005.



**Table 3.** Parameters and their various levels.

Key Factors	I Level	II Level	III Level
M	0.1	0.4	0.7
$\kappa$	3	4	5
$\beta_p$	3	4.5	6
Pr	7	8	9

**Table 4.** Taguchi L27 Experimental Design.

Experimental Runs	M	$\kappa$	$\beta_p$	Pr	Q
1	0.1	3	3	7	0.1
2	0.1	3	3	7	0.2
3	0.1	3	3	7	0.3
4	0.1	4	4.5	8	0.1
5	0.1	4	4.5	8	0.2
6	0.1	4	4.5	8	0.3
7	0.1	5	6	9	0.1
8	0.1	5	6	9	0.2
9	0.1	5	6	9	0.3
10	0.4	3	4.5	9	0.1
11	0.4	3	4.5	9	0.2
12	0.4	3	4.5	9	0.3
13	0.4	4	6	7	0.1
14	0.4	4	6	7	0.2
15	0.4	4	6	7	0.3
16	0.4	5	3	8	0.1
17	0.4	5	3	8	0.2
18	0.4	5	3	8	0.3
19	0.7	3	6	8	0.1
20	0.7	3	6	8	0.2
21	0.7	3	6	8	0.3
22	0.7	4	3	9	0.1
23	0.7	4	3	9	0.2
24	0.7	4	3	9	0.3
25	0.7	5	4.5	7	0.1
26	0.7	5	4.5	7	0.2
27	0.7	5	4.5	7	0.3

**Table 5.** Taguchi Results for Nusselt number.

Experimental Runs	Nu	Signal-to-Noise Ratio (SNR)
1	0.141373	-16.9927
2	0.13337	-17.4988
3	0.112723	-18.9597
4	0.142233	-16.94
5	0.136008	-17.3287
6	0.120702	-18.3657
7	0.142718	-16.9104
8	0.137548	-17.2309
9	0.1259	-17.9995
10	0.135357	-17.3704
11	0.120812	-18.3578
12	0.080144	-21.9226
13	0.137782	-17.2162
14	0.127996	-17.8561
15	0.105028	-19.5739
16	0.142766	-16.9075
17	0.136573	-17.2927
18	0.120496	-18.3805
19	0.12834	-17.8328
20	0.107913	-19.3385
21	0.05895	-24.5903
22	0.138648	-17.1617
23	0.127083	-17.9183
24	0.092806	-20.6485
25	0.138688	-17.1592
26	0.12908	-17.7828
27	0.105447	-19.5393

Residual plots for linear fit model are depicted in Fig. 26a and 26b. Figure 26a displays the normal probability plot which is aligned in the straight line predicting the fair precision of the model. Figure 26b gives the demonstration of residuals against the run number which has no proper patterned design. All these figures show the good fit depicting the precision of the model.

Figure 27 depicts that heat source parameter has large contribution of about 49.45% among the other parameters and Prandtl number has the least contribution of about 1.4% for optimisation. The error contribution is noted to be 18.85%.



**Table 6.** Response Table for S/Noise Ratio.

Level	M	$\kappa$	$\beta_p$	Pr	Q
1	-17.58	-19.21	-17.97	-18.06	-17.17
2	-18.32	-18.11	-18.31	-18.55	-17.84
3	-19.11	-17.69	-18.73	-18.39	-20.00
Delta	1.53	1.52	0.75	0.49	2.83
Rank	2	3	4	5	1

**Table 7.** Analysis of Variance for SN ratios.

Source	DF	Seq SS	Adj MS	F	P
M	2	10.499	5.2497	5.60	0.014
$\kappa$	2	11.045	5.5225	5.89	0.012
$\beta_p$	2	2.571	1.2855	1.37	0.282
Pr	2	1.115	0.5577	0.59	0.563
Q	2	39.351	19.6757	20.98	0.000
Residual Error	16	15.002	0.9376		
Total	26	79.584			

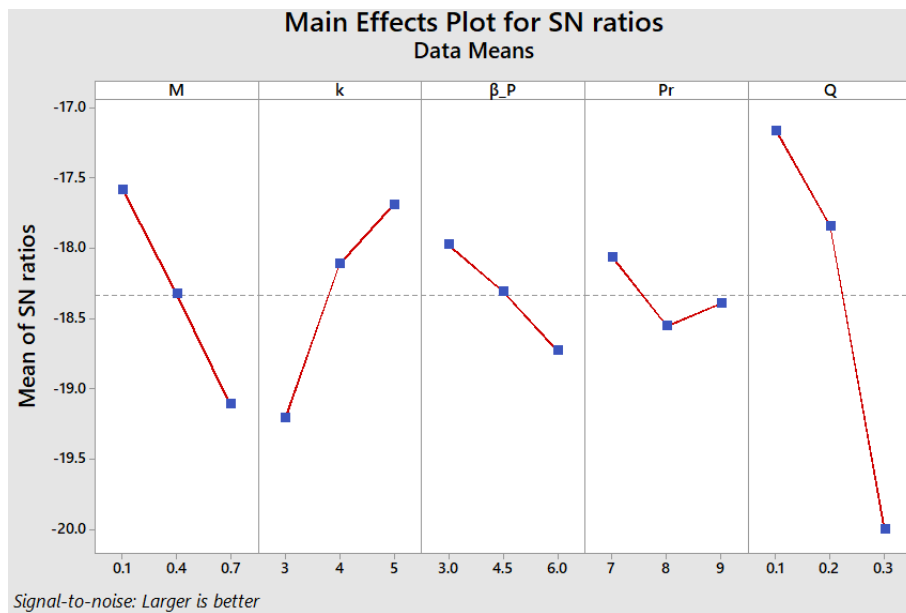


**Fig. 25.** Effect of key factors on Nusselt number.

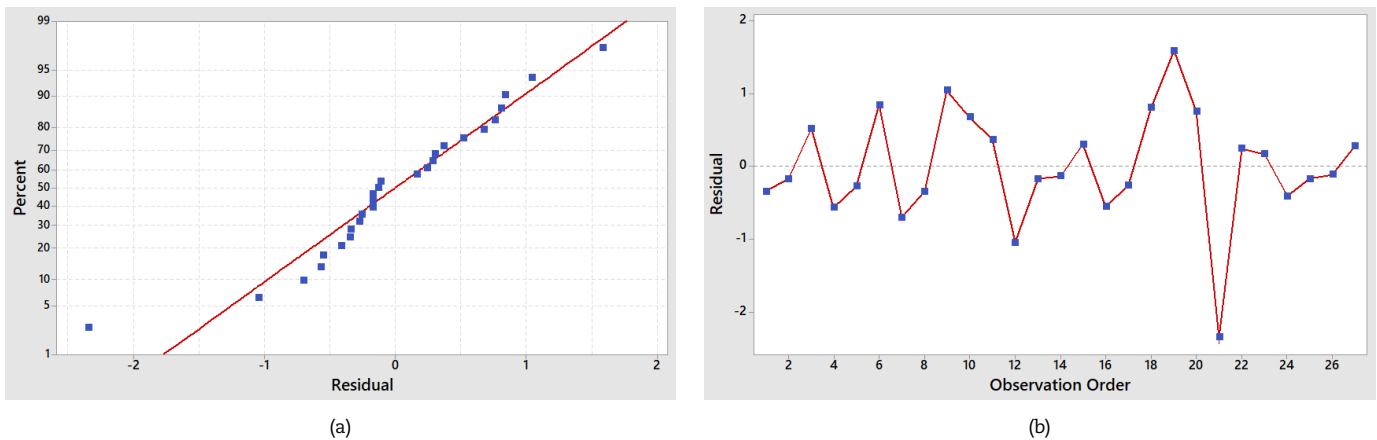


**Fig. 26.** (a) normal probability (b) residual versus run number.





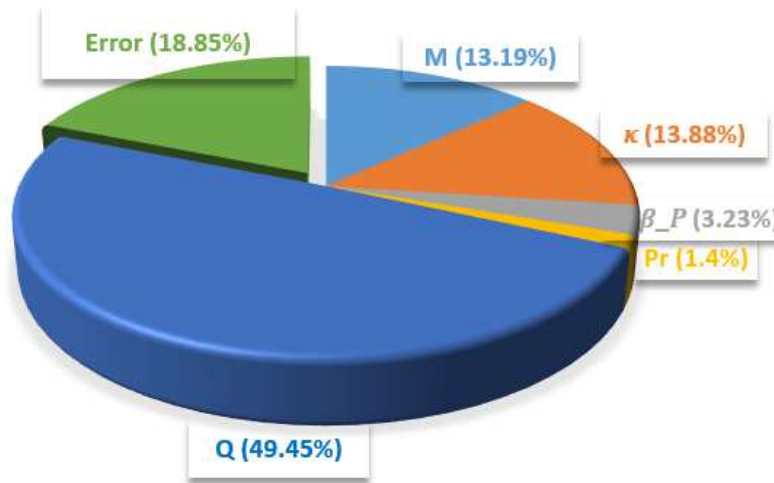


Fig. 27. Contribution of key factors on Nusselt number.

## 6. Concluding Reviews

The mathematical contemplation of the Prandtl nanofluid stream driven by a curved surface of stretching feature by considering an exponential heat propagation, Darcy-Forchheimer porous model, Joule heating, magnetic field, homo-heterogenic reactions and non-linear form of radiation. The surface boundary is enriched with convective and slip conditions. The configured flow equations are switched to simple equations by adopting similarity catalysts. Runge-Kutta-Fehlberg 4-5<sup>th</sup> order method is availed to portray graphical representations for the considered flow problem. The execution's key findings are:

- An enhancement in porous factor ( $\lambda$ ), Forchheimer number ( $Fr$ ) and velocity slip parameter ( $Ls$ ) impedes the velocity profile ( $f'(\eta)$ ) whereas the Prandtl fluid factor ( $\alpha_p$ ) and elastic factor ( $\beta_e$ ) fosters the same.
- The thermal distribution ( $\theta(\eta)$ ) encouraged by increasing radiation factor ( $Rd$ ), heat generation factor ( $Q$ ), and temperature difference factor ( $\theta_w$ ) whereas it depletes for increasing curvature parameter ( $\kappa$ ).
- The mass distribution ( $\phi(\eta)$ ) shows negative behaviour with burgeoning homogeneous-heterogeneous strengths ( $k_1$  and  $k_2$ ).
- Irreversibility for the flow is highest when Brinkmann number ( $Br$ ), Hartman number ( $M$ ) and Forchheimer number ( $Fr$ ).
- The fluid friction irreversibilities show supremacy for the Brinkmann number ( $Br$ ), Hartman number ( $M$ ) and Forchheimer number ( $Fr$ ).
- The rate of drag diminishes for upsurging magnitude of magnetic factor ( $M$ ) against factors upholding porosity ( $Fr$  and  $\lambda$ ).
- The Nusselt number is greatest when the Eckert number ( $Ec$ ) and radiation factor ( $Rd$ ) are least.
- Using Taguchi method, we may conclude that first level of magnetic parameter ( $M$ ), highest level of curvature element ( $\kappa$ ), starting level of elastic parameter ( $\beta_e$ ), Prandtl number ( $Pr$ ) and heat source parameter ( $Q$ ) produce an optimal arrangement to obtain maximum Nusselt number.
- Heat source parameter has large contribution of about 49.45% among the other and Prandtl number has the least contribution of about 1.4% for optimisation.

## Author Contributions

Numerical methodology conducted by A.R. Ajay Kumar, data analysis and methodology organized by F. Almeida, formal draft written by B. Nagaraja, conceptualization and methodology by Pradeep Kumar. Formal analysis and final review conducted by B.J. Gireesha. The manuscript was written through the contribution of all authors. All authors discussed the results, reviewed, and approved the final version of the manuscript.

## Acknowledgments

Not applicable.

## Conflict of Interest

The authors declared no potential conflicts of interest concerning the research, authorship, and publication of this article.

## Funding

The authors received no financial support for the research, authorship, and publication of this article.

## Data Availability Statements

The datasets generated and/or analyzed during the current study are available from the corresponding author on reasonable request.








## References


- [1] Sajid, M., Ali, N., Javed, T., Abbas, Z., Stretching a curved surface in a viscous fluid, *Chinese Physics Letters*, 27, 2010, 024703.
- [2] Hayat, T., Kiran, A., Imtiaz, M., Alsaedi, A., Hydromagnetic mixed convection flow of copper and silver water nanofluids due to a curved stretching sheet, *Results in Physics*, 6, 2016, 904-910.
- [3] Narla, V.K., Biswas, C., Rao, G.A., Entropy analysis of MHD fluid flow over a curved stretching sheet, *AIP Conference Proceedings*, 2246, 2020, 020099.
- [4] Nagaraja, B., Gireesha, B.J., Exponential space-dependent heat generation impact on MHD convective flow of Casson fluid over a curved stretching sheet with chemical reaction, *Journal of Thermal Analysis and Calorimetry*, 143, 2021, 4071-4079.
- [5] Usman, A.H., Hamisu, A., Khan, N.S., Rano, S.A., Maitama, M., Study of Heat and Mass Transfer in MHD Flow of Sutterby Nanofluid over a Curved Stretching Sheet with Magnetic Dipole and Effect, *Thai Journal of Mathematics*, 19, 2021, 1037-1055.
- [6] Khan, M.I., Alzahrani, F., Optimized framework for slip flow of viscous fluid towards a curved surface with viscous dissipation and Joule heating features, *Applied Mathematics and Computation*, 417, 2022, 126777.
- [7] Nadeem, S., Ijaz, S., Akbar, N.S., Nanoparticle analysis for blood flow of Prandtl fluid model with stenosis, *International Nano Letters*, 3, 2013, 1-13.
- [8] Khan, I., Malik, M.Y., Hussain, A., Salahuddin, T., Effect of homogenous-heterogeneous reactions on MHD Prandtl fluid flow over a stretching sheet, *Results in Physics*, 7, 2017, 4226-4231.
- [9] Hamid, M., Zubair, T., Usman, M., Khan, Z.H., Wang, W., Natural convection effects on heat and mass transfer of slip flow of time-dependent Prandtl fluid, *Journal of Computational Design and Engineering*, 6, 2019, 584-592.
- [10] Salmi, A., Madkhali, H.A., Ali, B., Nawaz, M., Alharbi, S.O., Alqahtani, A.S., Numerical study of heat and mass transfer enhancement in Prandtl fluid MHD flow using Cattaneo-Christov heat flux theory, *Case Studies in Thermal Engineering*, 33, 2022, 101949.
- [11] Patil, A.B., Patil, N.S., Patil, V.S., Humane, P.P., Rajput, G.R., Unsteady thermally radiative Prandtl fluid flow past a magnetized inclined porous stretching device with double-diffusion, viscous dissipation, and Joule heating, *Proceedings of the Institution of Mechanical Engineers, Part E: Journal of Process Mechanical Engineering*, 237, 2023, 762-770.
- [12] Hayat, T., Saif, R.S., Ellahi, R., Muhammad, T., Ahmad, B., Numerical study for Darcy-Forchheimer flow due to a curved stretching surface with Cattaneo-Christov heat flux and homogeneous-heterogeneous reactions, *Results in Physics*, 7, 2017, 2886-2892.
- [13] Gireesha, B.J., Nagaraja, B., Sindhu, S., Sowmya, G., Consequence of exponential heat generation on non-Darcy-Forchheimer flow of water-based carbon nanotubes driven by a curved stretching sheet, *Applied Mathematics and Mechanics*, 41, 2020, 1723-1734.
- [14] Muhammad, T., Rafique, K., Asma, M., Alghamdi, M., Darcy-Forchheimer flow over an exponentially stretching curved surface with Cattaneo-Christov double diffusion, *Physica A: Statistical Mechanics and its Applications*, 556, 2020, 123968.
- [15] Muhammad, R., Khan, M.I., Jameel, M., Khan, N.B., Fully developed Darcy-Forchheimer mixed convective flow over a curved surface with activation energy and entropy generation, *Computer Methods and Programs in Biomedicine*, 188, 2020, 105298.
- [16] Hayat, T., Qayyum, S., Alsaedi, A., Waqas, M., Simultaneous influences of mixed convection and nonlinear thermal radiation in stagnation point flow of Oldroyd-B fluid towards an unsteady convectively heated stretched surface, *Journal of Molecular Liquids*, 224, 2016, 811-817.
- [17] Patel, H.R., Singh, R., Thermophoresis Brownian motion and non-linear thermal radiation effects on mixed convection MHD micropolar fluid flow due to nonlinear stretched sheet in porous medium with viscous dissipation joule heating and convective boundary condition, *International Communications in Heat and Mass Transfer*, 107, 2019, 68-92.
- [18] Raza, R., Mabood, F., Naz, R., Abdelsalam, S.I., Thermal transport of radiative Williamson fluid over stretchable curved surface, *Thermal Science and Engineering Progress*, 23, 2021, 100887.
- [19] Algehyne, E.A., Aldhabani, M.S., Saeed, A., Dawar, A., Kumam, P., Mixed convective flow of Casson and Oldroyd-B fluids through a stratified stretching sheet with nonlinear thermal radiation and chemical reaction, *Journal of Taibah University for Science*, 16, 2022, 193-203.
- [20] Imtiaz, M., Hayat, T., Alsaedi, A., Hobiny, A., Homogeneous-heterogeneous reactions in MHD flow due to an unsteady curved stretching surface, *Journal of Molecular Liquids*, 221, 2016, 245-253.
- [21] Pal, D., Mandal, G., Effects of aligned magnetic field on heat transfer of water-based carbon nanotubes nanofluid over a stretching sheet with homogeneous-heterogeneous reactions, *International Journal of Ambient Energy*, 42, 2021, 1-13.
- [22] Imtiaz, M., Mabood, F., Hayat, T., Alsaedi, A., Homogeneous-heterogeneous reactions in MHD radiative flow of second grade fluid due to a curved stretching surface, *International Journal of Heat and Mass Transfer*, 145, 2019, 118781.
- [23] Ashraf, M.B., Ul Haq, S., The convective flow of Carreau fluid over a curved stretching surface with homogeneous-heterogeneous reactions and viscous dissipation, *Waves in Random and Complex Media*, 32, 2022, 1-15.
- [24] Manjunatha, S., Puneeth, V., Gireesha, B.J., Chamkha, A.J., Theoretical Study of Convective Heat Transfer in Ternary Nanofluid Flowing past a Stretching Sheet, *Journal of Applied and Computational Mechanics*, 8, 2022, 1279-1286.
- [25] Sharma, R.P., Shaw, S., MHD Non-Newtonian Fluid Flow past a Stretching Sheet under the Influence of Non-linear Radiation and Viscous Dissipation, *Journal of Applied and Computational Mechanics*, 8, 2022, 949-961.
- [26] Felicita, A., Berrehal, H., Venkatesh, P., Gireesha, B.J., Sowmya, G., Slip flow of Walter's B liquid through the channel possessing stretched walls by employing optimal homotopy asymptotic method (OHAM), *Journal of Molecular Liquids*, 353, 2022, 118731.
- [27] Nagaraja, B., Ajaykumar, A.R., Felicita, A., Pradeep, K., Rudraswamy, N.G., Non-Darcy-Forchheimer flow of Casson-Williamson nanofluid on melting curved stretching sheet influenced by magnetic dipole, *ZAMM-Journal of Applied Mathematics and Mechanics*, 2023, <https://doi.org/10.1002/zamm.202300134>.
- [28] Animasaun, I.L., Adebile, E.A., Fagbade, A.I., Casson fluid flow with variable thermo-physical property along exponentially stretching sheet with suction and exponentially decaying internal heat generation using the homotopy analysis method, *Journal of the Nigerian Mathematical Society*, 35, 2016, 1-17.
- [29] Zia, Q.M., Ullah, I., Waqas, M., Alsaedi, A., Hayat, T., Cross diffusion and exponential space dependent heat source impacts in radiated three-dimensional (3D) flow of Casson fluid by heated surface, *Results in Physics*, 8, 2018, 1275-1282.
- [30] Kumar, A., Reddy, J.V.R., Sugunamma, V., Sandeep, N., Impact of cross diffusion on MHD viscoelastic fluid flow past a melting surface with exponential heat source, *Multidiscipline Modelling in Materials and Structures*, 14, 2018, 999-1016.
- [31] Nagaraja, B., Gireesha, B.J., Soumya, D.O., Almeida, F., Characterization of MHD convective flow of Jeffrey nanofluid driven by a curved stretching surface by employing Darcy-Forchheimer law of porosity, *Waves in Random and Complex Media*, 2022, <https://doi.org/10.1080/17455030.2021.2020933>.
- [32] Kumar, P., Nagaraja, B., Almeida, F., Ajaykumar, A.R., Al-Mdallal, Q., Jarad, F., Magnetic dipole effects on unsteady flow of Casson-Williamson nanofluid propelled by stretching slippery curved melting sheet with buoyancy force, *Scientific Reports*, 13, 2023, 12770.
- [33] Bejan, A., Entropy generation minimization: The new thermodynamics of finite-size devices and finite-time processes, *Journal of Applied Physics*, 79, 1996, 1191-1218.
- [34] Hayat, T., Qayyum, S., Alsaedi, A., Ahmad, B., Entropy generation minimization: Darcy-Forchheimer nanofluid flow due to curved stretching sheet with partial slip, *International Communications in Heat and Mass Transfer*, 111, 2020, 104445.
- [35] Almeida, F., Venkatesh, P., Gireesha, B.J., Nagaraja, B., Eshwarappa, K.M., Compressed flow of hybridized nanofluid entwined between Two rotating plates exposed to radiation, *Journal of Nanofluids*, 10, 2021, 186-199.
- [36] Mishra, S.R., Sharma, R.P., Tinker, S., Panda, G.K., Impact of Slip and the Entropy Generation in a Darcy-Forchhimer Nanofluid Past a Curved Stretching Sheet with Heterogeneous and Homogenous Chemical Reactions, *Journal of Nanofluids*, 11, 2022, 48-57.
- [37] Almeida, F., Gireesha, B.J., Venkatesh, P., Ramesh, G.K., Intrinsic irreversibility of Al<sub>2</sub>O<sub>3</sub>-H<sub>2</sub>O nanofluid Poiseuille flow with variable viscosity and convective cooling, *International Journal of Numerical Methods for Heat & Fluid Flow*, 31, 2022, 2042-2063.
- [38] Sheikholeslami, M., Efficacy of porous foam on discharging of phase change material with inclusion of hybrid nanomaterial, *Journal of Energy Storage*, 62, 2023, 106925.



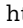
- [39] Sheikholeslami, M., Numerical investigation for concentrated photovoltaic solar system in existence of paraffin equipped with MWCNT nanoparticles, *Sustainable Cities and Society*, 99, 2023, 104901.
- [40] Sheikholeslami, M., Numerical investigation of solar system equipped with innovative turbulator and hybrid nanofluid, *Solar Energy Materials and Solar Cells*, 243, 2022, 111786.
- [41] Upreti, H., Pandey, A.K., Kumar, M., Makinde, O.D., Darcy-Forchheimer flow of CNTs-H<sub>2</sub>O nanofluid over a porous stretchable surface with Xue model, *International Journal of Modern Physics B*, 37, 2023, 2350018.
- [42] Upreti, H., Bartwal, P., Pandey, A.K., Makinde, O.D., Heat transfer assessment for Au-blood nanofluid flow in Darcy-Forchheimer porous medium using induced magnetic field and Cattaneo-Christov model, *Numerical Heat Transfer, Part B: Fundamentals*, 2023, 1-17.
- [43] Nayak, M.K., Shaw, S., Khan, M.I., Makinde, O.D., Yu-Ming, C., Khan, S.U., Interfacial layer and shape effects of modified Hamilton's Crosser model in entropy optimized Darcy-Forchheimer flow, *Alexandria Engineering Journal*, 60, 2021, 4067-4083.
- [44] Tadesse, F.B., Makinde, O.D., Enyadene, L.G., Hydromagnetic stagnation point flow of a magnetite ferrofluid past a convectively heated permeable stretching/shrinking sheet in a Darcy-Forchheimer porous medium, *Sadhana*, 46, 2021, 115.
- [45] Shaw, S., Dogonchi, A.S., Nayak, M.K., Makinde, O.D., Impact of entropy generation and nonlinear thermal radiation on Darcy-Forchheimer flow of MnFe<sub>2</sub>O<sub>4</sub>-Casson/water nanofluid due to a rotating disk: Application to brain dynamics, *Arabian Journal for Science and Engineering*, 45, 2020, 5471-5490.
- [46] Nagaraja, B., Felicita, A., Ali, Y., Pradeep, K., Ajaykumar, A.R., Al-Mdallal, Q., Empirical study for Nusselt number optimization for the flow using ANOVA and Taguchi method, *Case Studies in Thermal Engineering*, 50, 2023, 103505.
- [47] Pradeep, K., Ajaykumar, A.R., Felicita, A., Nagaraja, B., Qasem, Al-M., Youssef El-K., Model Designed to Acquire an Optimized Performance Implementing L27 Orthogonal Array for the Prandtl Fluid Flow Maneuvering Grey Relational Theory, *International Journal of Thermofluids*, 20, 2023, 100490.
- [48] Prakash, D., Kumar, S., Muthamilselvan, M., Al-Mdallal Q.M., Heat transfer enhancement in a nanofluid saturated porous medium with cross diffusion and nonequilibrium: A regression approach, *Numerical Heat Transfer, Part A: Applications*, 83, 2023, 1408-1420.
- [49] Barman, T., Roy, S., Chamkha, A.J., Magnetized Bi-convective Nanofluid Flow and Entropy Production Using Temperature-sensitive Base Fluid Properties: A Unique Approach, *Journal of Applied and Computational Mechanics*, 8, 2022, 1163-1175.
- [50] Sankar, M., Swamy, H.A.K., Al-Mdallal, Q., Wakif, A., Non-Darcy nanoliquid buoyant flow and entropy generation analysis in an inclined porous annulus: Effect of source-sink arrangement, *Alexandria Engineering Journal*, 68, 2023, 239-261.
- [51] Almeida, F., Gireesha, B.J., Venkatesh, P., Magneto-hydrodynamic flow of a micropolar nanofluid in association with Brownian motion and thermophoresis: Irreversibility analysis, *Heat Transfer*, 52, 2023, 2032-2055.
- [52] Felicita, A., Pradeep, K., Nagaraja, B., Gireesha, B.J., Venkatesh, P., Parametric optimisation of entropy using sensitivity analysis and response surface methodology for the compressed flow of hybrid nanoliquid in a stretchable channel, *Pramana*, 97, 2023, 159.
- [53] Singh, V.D., Hussain, M.M., Experimental investigation and optimization of coefficient of friction of brass sheet metal using Taguchi technique, *AIP Conf. Proc.*, 2754, 2023, 100003.
- [54] Jou, Y.T., Lin, W.T., Lee, W.C., Yeh, T.M., Integrating the Taguchi method and response surface methodology for process parameter optimization of the injection molding, *Applied Mathematics & Information Sciences*, 8(3), 2014, 1277.
- [55] Rana, P., Gupta, S., Gupta, G., FEM computations and Taguchi optimization in nonlinear radiative MHD MWCNT-MgO/EG hybrid nanoliquid flow and heat transfer over a 3D wedge surface, *Case Studies in Thermal Engineering*, 41, 2023, 102639.
- [56] Rana, P., Gupta, S., Gupta, G., Optimization of heat transfer by nonlinear thermal convection flow past a solid sphere with Stefan blowing and thermal slip using Taguchi method, *International Communications in Heat and Mass Transfer*, 141, 2023, 106580.

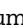
## ORCID iD

B. Nagaraja  <https://orcid.org/0000-0002-8081-9950>

B.J. Gireesha  <https://orcid.org/0000-0002-4761-1082>

F. Almeida  <https://orcid.org/0000-0003-2136-8771>

P. Kumar  <https://orcid.org/0000-0002-4875-5387>

A.R. Ajaykumar  <https://orcid.org/0009-0007-1849-7747>



© 2023 Shahid Chamran University of Ahvaz, Ahvaz, Iran. This article is an open access article distributed under the terms and conditions of the Creative Commons Attribution-NonCommercial 4.0 International (CC BY-NC 4.0 license) (<http://creativecommons.org/licenses/by-nc/4.0/>).

**How to cite this article:** Nagaraja B., Gireesha B.J., Almeida F., Kumar P., Ajaykumar A.R. Entropy Analysis of Darcy-Forchheimer Model of Prandtl Nanofluid over a Curved Stretching Sheet and Heat Transfer Optimization by ANOVA-Taguchi Technique, *J. Appl. Comput. Mech.*, 10(2), 2024, 287-303. <https://doi.org/10.22055/jacm.2023.44524.4229>

**Publisher's Note** Shahid Chamran University of Ahvaz remains neutral with regard to jurisdictional claims in published maps and institutional affiliations.

